

Chiral spin ordering of electron gas in solids with broken time reversal symmetry

K. S. Denisov,^{1,2,*} I. V. Rozhansky,^{1,2} N. S. Averkiev,¹ and E. Lähderanta²

¹*Ioffe Institute, 194021 St.Petersburg, Russia*

²*Lappeenranta-Lahti University of Technology, FI-53851 Lappeenranta, Finland*

In this work we manifest that an electrostatic disorder in conducting systems with broken time reversal symmetry universally leads to a chiral ordering of the electron gas giving rise to skyrmion-like textures in spatial distribution of the electron spin density. We describe a microscopic mechanism underlying the formation of the equilibrium chiral spin textures in two-dimensional systems with spin-orbit interaction and exchange spin splitting. We have obtained analytical expressions for spin-density response functions and have analyzed both local and non-local spin response to electrostatic perturbations for systems with parabolic-like and Dirac electron spectra. With the proposed theory we come up with a concept of controlling spin chirality by electrical means.

The concept of spin chirality constitutes a substantial part of modern condensed matter physics. It is widely applied for strongly correlated electron systems¹⁻⁴ when interpreting the fractional statistics⁵⁻⁷, or chiral spin liquids⁸⁻¹¹ in terms of an effective gauge field. Remarkably, a finite spin chirality induces a gauge invariant magnetic flux, which is an experimentally observable quantity¹. It was shown that the chirality driven magnetic field affects electron transport in the very same way as the ordinary magnetic field does^{12,13} leading to the Hall response, the phenomenon currently referred as the topological Hall effect¹⁴⁻¹⁶. Naturally, to get an experimental access to the variety of spin chirality driven phenomena an efficient tool for creating chiral spin order is needed. One way towards this goal is to focus on materials possessing exotic spin textures, such as magnetic skyrmions¹⁷⁻²⁰, or merons²¹. Still, exploring the physical mechanisms behind the emergence of spin chirality in solids remains challenging and is of high fundamental interest.

In this Letter we show that in systems with broken time reversal symmetry (\mathcal{T} -symmetry) a chiral spin order of electron gas is universally induced by an electrostatic disorder, which is an inherent property of any real solid. We argue that numerous crystal imperfections, such as residue impurities or surface defects appear to be a source of local chiral spin ordering in the electron gas. This effect is more pronounced for an electron gas with stronger spin-orbit interaction (SOI). Naturally, various magnetic systems such as magnetic topological insulators (TI)²²⁻²⁵, Rashba magnetic layers²⁶⁻²⁹ or dilute magnetic semiconductors (DMS)³⁰⁻³⁵ are in fact flooded by chiral spin textures pinned to structural defects. This effect opens up a novel concept of an experimental research of spin chirality driven phenomena.

In our work we focus on two-dimensional degenerate electron gas (2DEG) with a spin-orbit interaction and an exchange spin splitting. We introduce an effective 'magnetic field' acting on an electron spin:

$$\mathbf{B}_k = (\lambda k \cos(\chi\varphi_k + \gamma), \lambda k \sin(\chi\varphi_k + \gamma), h), \quad (1)$$

where $\mathbf{k} = (k, \varphi_k)$ is a 2D momentum with magnitude k and polar angle φ_k . The parameter $h > 0$ describes the out-of-plane component leading to the carrier spin

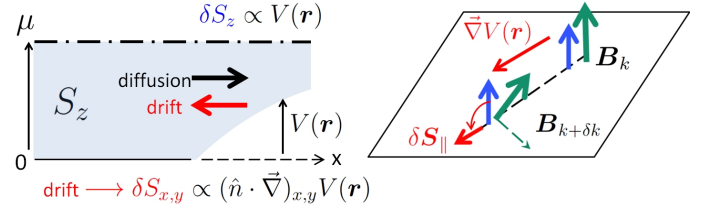


FIG. 1: The physical picture behind the emergence of an equilibrium chiral spin pattern of the electron gas. The in-plane spin arises from the precession due to drift electron flow.

splitting at $k = 0$, it is thus responsible for the violation of \mathcal{T} -symmetry. The in-plane components of \mathbf{B}_k represent linear in k terms due to SOI, λ is the SOI coupling constant. The SOI parameters $\chi = \pm 1$ (helicity) and γ (vorticity) cover different types of the SOI interaction.

Let us further assume an electrostatic disorder due to various defects present in the system. When \mathcal{T} -symmetry is broken the spatial distribution of the equilibrium electron spin density follows the inhomogeneity of the electrostatic potential $V(\mathbf{r})$. Indeed, at $h \neq 0$ there is a nonzero electron spin polarization directed perpendicular to the motion plane (z -axis). A local shift of $V(\mathbf{r})$ leads to a spatial redistribution of electrons and, hence, to the change of δS_z . When SOI is present ($\lambda \neq 0$) the in-plane components of the spin density $\delta S_{x,y}$ appear as well, so the induced spin response $\delta \mathbf{S}$ acquires a chiral spatial pattern forming skyrmion-like spin textures.

Let us notice that the mechanics behind the appearance of $\delta S_{x,y}$ in response to an electrostatic potential has a peculiar character, and it differs from that for δS_z . Since there is no net in-plane spin polarization at a spatially uniform electrostatic potential, $\delta S_{x,y}$ appears only due to its gradient. One can consider the following quasiclassical picture, see Fig.1. An electron with initial momentum \mathbf{k} and spin \mathbf{S}_k co-aligned with the direction of \mathbf{B}_k moves along a certain trajectory. Due to the electrostatic potential gradient $\vec{\nabla}V(\mathbf{r})$ the carrier momentum is changed $\mathbf{k} + \delta\mathbf{k}$, thus changing the tilt of the magnetic field $\mathbf{B}_{k+\delta k}$, which in-plane components are coupled with momentum. This process triggers the precession of elec-

tron spin around the new direction of the magnetic field creating an excessive in-plane spin density. In the thermodynamic equilibrium there is no net current as the drift and diffusion electron flows are compensated everywhere. However, the in-plane components of the spin density still appear because the drift flow is associated with a change of the electron momentum.

The emergence of the spin textures due to spatial variation of the electrostatic potential is described by static spin-density response functions:

$$\mathcal{F}_\alpha(\mathbf{q}) = \sum_{k,s,s'} \langle u_k^s | \hat{S}_\alpha | u_{k+q}^{s'} \rangle \langle u_{k+q}^{s'} | u_k^s \rangle \frac{f_k^s - f_{k+q}^{s'}}{\varepsilon_k^s - \varepsilon_{k+q}^{s'} + i0}, \quad (2)$$

where \hat{S}_α is a spin operator for $\alpha = (x, y, z)$ axis, index $s = \pm$ denotes two electron subbands, ε_k^s and $|u_k^s\rangle$ are the energy and the Bloch amplitude of an electron in state (\mathbf{k}, s) , f_k^s is the equilibrium distribution function. Using the functions $\mathcal{F}_\alpha(\mathbf{q})$ one can analyze the spin density $\delta\mathbf{S}(\mathbf{r})$ emerging in 2DEG in the vicinity of a doping center or a defect characterized by a potential $V(\mathbf{r})$:

$$\delta\mathbf{S}_\alpha(\mathbf{r}) = \int \frac{d\mathbf{q}}{(2\pi)^2} e^{i\mathbf{q}\mathbf{r}} \mathcal{F}_\alpha(\mathbf{q}) V(\mathbf{q}), \quad (3)$$

where $V(\mathbf{q})$ is the Fourier transform of $V(\mathbf{r})$, the electron-electron interaction is neglected. In particular, the functions $\mathcal{F}_\alpha(\mathbf{q})$ allow us to identify whether the spin response is local or extends beyond the localization radius of the potential due to the wave properties of 2DEG.

Let us point out a few general features of the spin response in the considered model. As has been mentioned above, z -component of spin is analogous to the electron density, so if there is no spatial dispersion δS_z locally couples with the potential $\delta S_z(\mathbf{r}) = \varkappa_z V(\mathbf{r})$. The coefficient \varkappa_z is given by a product of the electron density of states and z -projection of spin taken at the Fermi energy. On the contrary, the in-plane spin components driven by the precession mechanism illustrated by Fig. 1 are induced by the gradient of $V(\mathbf{r})$. In the case of a local response this coupling takes the form $\delta S_{x,y} = \varkappa_{\parallel} (\hat{n} \cdot \vec{\nabla})_{x,y} V(\mathbf{r})$, where \hat{n} is a unitary matrix determined by SOI type, and the coefficient \varkappa_{\parallel} is determined by a carrier spectrum. Since the Fourier transform of $\vec{\nabla} V(\mathbf{r})$ is $i\mathbf{q}V(\mathbf{q})$, we conclude that $\mathcal{F}_{x,y}(\mathbf{q})$ are purely imaginary, we present them as

$$\mathcal{F}_{x,y}(\mathbf{q}) = i (\hat{n} \mathbf{e}_q)_{x,y} \mathcal{F}_{\parallel}(q), \quad (4)$$

where the real function $\mathcal{F}_{\parallel}(q)$ depends on the absolute value of q , $\mathbf{e}_q = \mathbf{q}/q$. Naturally, $\mathcal{F}_{\parallel}(q) \propto q$ at $q \rightarrow 0$.

As soon as there is some spatial inhomogeneity of crystalline structure the electron gas acquires a local spin chirality. For an axially symmetric potential $V(r)$ the

excessive spin density $\delta\mathbf{S}(\mathbf{r})$ profile has a shape:

$$\delta\mathbf{S}(\mathbf{r}) = \begin{pmatrix} \delta S_{\parallel}(r) \cos(\chi\varphi_r + \gamma') \\ \delta S_{\parallel}(r) \sin(\chi\varphi_r + \gamma') \\ \delta S_z(r) \end{pmatrix}, \quad (5)$$

$$\delta S_{z,\parallel}(r) = \int \frac{qdq}{2\pi} J_{0,1}(qr) \mathcal{F}_{z,\parallel}(q) V(q),$$

where r, φ_r are the polar coordinates of a radius vector, $\delta S_{\parallel}, \delta S_z$ depend on r , $J_{0,1}$ are Bessel's functions of the zeroth and first order, respectively, $\gamma' = \gamma + \pi/2$. The emerging chiral spin cloud is similar to a skyrmion for $\chi = 1$, or to an antiskyrmion for $\chi = -1$. The fact that the helicity γ' of the real space spin rotation is shifted by $\pi/2$ with respect to γ in k -space reflects the spin precession mechanism.

The details of chiral spin response naturally depend on a carrier band structure ε_k^{\pm} . Below we calculate $\mathcal{F}_{z,\parallel}(q) = \mathcal{F}_{z,\parallel}^+ + \mathcal{F}_{z,\parallel}^-$, which is a sum of the responses of two subbands (see Supplementary materials), and analyze the spin response for parabolic-like and Dirac electron spectra.

Parabolic-like spectrum. Let us assume the following Hamiltonian H_k and the energy spectrum ε_k^{\pm} :

$$H_k = \frac{k^2}{2m} - \mathbf{B}_k \cdot \hat{\sigma}, \quad (6)$$

$$\varepsilon_k^{\pm} = \frac{k^2}{2m} \mp B_k, \quad B_k = \sqrt{h^2 + (\lambda k)^2},$$

where m is the effective mass in the absence of the field B_k (we assume $\hbar=1$). In this paper we take the parameter $\xi = m\lambda^2/h < 1$. The spectrum of the system is shown in Fig. 2a, the color within each subband indicates the magnitude of $\zeta_s = \lambda k_s/h$, which has a meaning of spin inclination into the plane of the carrier motion (blue color corresponds to $\zeta_s \ll 1$, red color indicates $\zeta_s \gg 1$).

We have obtained analytic expressions for the spin-density response functions $\mathcal{F}_{z,\parallel}$ with the spectrum given by Eq. 6. As the formulas are rather cumbersome, we provide them in the Supplementary Materials. Importantly, $\mathcal{F}_{z,\parallel}^{\pm}$ within each subband are decomposed onto a sum of intra- and interband contributions $\mathcal{F}_{z,\parallel}^{\pm} = \mathcal{F}_{z,\parallel}^{\pm\pm} + \mathcal{F}_{z,\parallel}^{\pm\mp}$ with the interband terms exhibiting an additional coupling $\mathcal{F}_z^{\pm\mp}(q) = (2m\lambda/q) \mathcal{F}_{\parallel}^{\pm\mp}(q)$.

Let us firstly consider the local coupling regime, when $\delta S_{x,y}(\mathbf{r}) = \varkappa_{\parallel} (\hat{n} \cdot \vec{\nabla})_{x,y} V(\mathbf{r})$ and $\delta S_z(\mathbf{r}) = \varkappa_z V(\mathbf{r})$. The coefficients $\varkappa_{z,\parallel} = \varkappa_{z,\parallel}^+ + \varkappa_{z,\parallel}^-$ found from the limiting behavior of $\mathcal{F}_{z,\parallel}^{\pm}$ at $q \rightarrow 0$ are given in Supplementary Materials. As already mentioned, $\varkappa_{z,\parallel}^{\pm}$ is the product of the density of states and the spin z -projection at the Fermi energy μ . The dependence of $\varkappa_{z,\parallel}$ on μ is shown in Fig 2b,c. We note that nonzero spin response is observed only when the upper subband is free of electrons ($\mu < h$). This result is an inherent property of the considered model; the background spin density $S_z^0 = (mh/4\pi)$ remains constant at $\mu > h$.

As follows from the explicit expressions for $\mathcal{F}_{z,\parallel}^\pm$, the local coupling regime occurs when the Fourier components of $V(\mathbf{q})$ are localized within $q \ll \min[k_\pm, a_0^{-1}]$, where $a_0 = \lambda/2h$. For these values the response functions \mathcal{F}_z , $\mathcal{F}_{\parallel}/q$ have a weak dependence on q , which means no spatial dispersion and, thus, the absence of non-locality in the response. Note, that, apart from the Fermi wavevector k_\pm , there is a second spatial scale $a_0 = \lambda/2h$, which controls the spatial dispersion of the spin response. This scale is associated with the precession mechanism for the in-plane spin generation.

Naturally, a more interesting spin physics takes place when the effects of spatial dispersion come to the fore. We first consider the case when only the (+) subband is populated ($-h < \mu < h$). The dependence of $\mathcal{F}_{z,\parallel}^+$, and its partial contributions $\mathcal{F}_{z,\parallel}^{\pm\pm}$ on $q/2k_+$ are shown in Fig. 3(a,b). As we have discussed above, the response functions at $q \rightarrow 0$ behave as $\mathcal{F}_z^+ \sim q^0$, $\mathcal{F}_{\parallel}^+ \sim q^1$. Another general trend is that the intra- $\mathcal{F}_{z,\parallel}^{\pm\pm}$ and interband $\mathcal{F}_{z,\parallel}^{\mp\mp}$ terms have an opposite sign and, thus, tend to cancel each other. The spatial profile $\delta S_{z,\parallel}(r)$ induced around a repulsive short range potential $V(r) = \alpha_0 \delta(\mathbf{r})$ is shown in Fig. 3c. The largest spin response appears within the Fermi wavelength ($2k_+ r \lesssim 2$). Going away from the center $S_{z,\parallel}(r)$ decrease exhibiting the Friedel oscillations with the period $2k_+$ (see inset in Fig.3).

Let us now consider the case $\mu > h$ when both spin subbands are populated. Although the local spin response is absent in this case ($\varkappa_{z,\parallel} = 0$), the effect of spatial dispersion restores a chiral spin pattern. Shown in Fig. 3(d-g) are the calculated spin response functions $\mathcal{F}_{z,\parallel}^\pm(q)$. We note that the intraband terms $\mathcal{F}_{z,\parallel}^{\pm\pm}$ for both subbands exhibit a single spike at $q = 2k_\pm$. What is more interesting is the double-spike structure of the interband terms $\mathcal{F}_{z,\parallel}^{\mp\mp}$ driven by two nesting vectors connecting two distinct subbands of the Fermi surface. The presence of the two different spatial scales k_\pm along with a complex structure of interband transitions lead to quite a peculiar spin response in the real space. In Fig. 3h,i we demonstrate $\delta S_{z,\parallel}(r)$ for the short range potential $V(q) = \alpha_0$. The spatial scale is given in units of $x = k_F r$, where k_F is the averaged Fermi wavevector. The Friedel oscillations clearly visible at large distances from the centre $x \gg 1$ are now formed by the superposition of oscillations with different spatial periods.

Dirac spectrum. Let us further consider the case of Hamiltonian with Dirac spectrum:

$$H_{\mathbf{k}} = -\mathbf{B}_{\mathbf{k}} \cdot \hat{\boldsymbol{\sigma}}, \quad \varepsilon_{\mathbf{k}}^\pm = \mp \sqrt{h^2 + (\lambda \mathbf{k})^2}. \quad (7)$$

This model describes, for example, chiral surface states of a 3D TI (the SOI parameters are $\chi = 1$, $\gamma = \pi$). Shown in Fig. 4a is the spectrum (7), which consists of two nearly linear bands separated by the gap $2h$. The fundamental difference from the previously considered parabolic-like spectrum is the additional electron-hole symmetry (\mathcal{C} -symmetry), which modifies the electron gas response to

external perturbations³⁶⁻³⁹.

Let us put the Fermi energy $\mu > 0$ above the charge neutrality point, so the lower (+) band is completely filled while the upper (-) band is filled partially. Our calculations show that the filled lower subband does not contribute to the response of z spin component ($\mathcal{F}_z^+ = 0$), while for the upper (-) subband the spin response function is the conventional 2D Lindhard function:

$$\mathcal{F}_z^-(q) = \frac{m_g}{4\pi} \left(1 - \Theta[q - 2k_-] \sqrt{1 - 4k_-^2/q^2} \right), \quad (8)$$

where $m_g = h/\lambda^2$ is an effective mass due to the spectrum gap, $k_- = \sqrt{\mu^2 - h^2}/\lambda$ is the Fermi wavevector. This result is rather interesting as the Lindhard function usually describes the susceptibility of a system with simple parabolic spectrum.

Another important feature of \mathcal{F}_z^- given by (8) is that its magnitude does not depend on the Fermi energy μ . This is in contrast with the parabolic-like case, where the increase of μ leads to the suppression of spin response according to $\mathcal{F}_z^\pm \propto 1/\zeta_\pm$ at $\zeta_\pm \gg 1$. This effect is due to the density of states, which for the Dirac spectrum takes the form $\nu_- = B_k/2\pi\lambda^2$. Upon the increase of the Fermi energy the suppression of spin z -projection (which is $h/2B_k \propto 1/\zeta_-$ at $\mu \gg h$) is exactly compensated by the increase of $\nu_-(\mu)$. For instance, considering the local coupling regime $\delta S_z = \varkappa_z V(\mathbf{r})$ the spin response is explicitly determined by a product $\varkappa_z^- = \nu_-(\mu) \cdot n_k/2 = (m_g/4\pi)$ independent of μ .

The in-plane spin response also exhibits a number of peculiar features. For the functions $\mathcal{F}_{\parallel}^\pm(q)$ we obtained:

$$\mathcal{F}_{\parallel}^+(q) = \frac{m_g}{4\pi} \tan^{-1}(qa_0), \quad (9)$$

$$\mathcal{F}_{\parallel}^- = -\mathcal{F}_{\parallel}^+ + \frac{m_g}{4\pi} \Theta[q - 2k_-] \tan^{-1} \left(a_0 \sqrt{\frac{q^2 - 4k_-^2}{1 + \zeta_-^2}} \right).$$

We note that there is a non-zero spin response from the completely filled (+) subband, and that $\mathcal{F}_{\parallel}^+/q$ remains finite even at $qa_0 \ll 1$. This is an unusual behavior, since no density response of (+) subband can be induced in this case. Indeed, the interband transitions underlying the change of electron density are suppressed for a smooth potential $qa_0 \ll 1$ due to the finite band gap $2h$. On the contrary, the in-plane spin response originates from the spin precession driven by a drift electron flow, which remains finite in \mathcal{C} -symmetry systems even with gaped spectrum due to the Klein tunneling.

Considering the in-plane spin response from the upper (-) subband we note that the function $\mathcal{F}_{\parallel}^-(q)$ given by Eq. 9 contains both the μ -independent term opposite to that of (+) subband, and a μ -aware contribution responsible for the Friedel's oscillations with the spatial period $2k_-$. The in-plane spin response function $\mathcal{F}_{\parallel} = \mathcal{F}_{\parallel}^+ + \mathcal{F}_{\parallel}^-$ and its partial components $\mathcal{F}_{\parallel}^{\pm\pm}$ are shown in Fig. 4b. The contributions of (\pm) subbands cancel each other at

$q < 2k_-$ and \mathcal{F}_\parallel turns to zero. Therefore, no in-plane spin response is induced by a long-range electrostatic perturbation when the Fermi level is in the upper subband.

The non-local spin response is also modified due to \mathcal{C} -symmetry. As can be seen in Fig. 4b the function $\mathcal{F}_\parallel(q) = \mathcal{F}_\parallel^+ + \mathcal{F}_\parallel^-$ saturates at $q \gg k_-$ instead of going to zero. However, as discussed above, the in-plane spin density responds to the potential gradient, so it is $\mathcal{F}_\parallel(q)/q$ which has the physical meaning and it indeed decays as $1/q$ when $\mathcal{F}_\parallel(q)$ saturates. In Fig. 4c we show the spatial spin pattern $\delta S_{z,\parallel}$ induced by a short-range potential $V(q) = \alpha_0 \exp[-(qa/2)^2]$, a is a potential radius. It is worth mentioning that the magnitude of the in-plane spin response δS_\parallel in the vicinity of a defect is far larger than in the parabolic spectra case due to the saturation of $\mathcal{F}_\parallel(q)$. This finding emphasizes a particularly high susceptibility of chiral spin pattern in response to an electrostatic disorder in systems with Dirac spectrum.

Discussion. Our study suggests that the emergence of chiral spin textures driven by an electrostatic disorder is a universal phenomena. The obtained results are applicable to a variety of experimentally studied systems, such as DMS^{34,40}, thin films of ferromagnets^{26,27}, Bi₂Se₃ doped by magnetic impurities^{24,25,41,42}, or due to the proximity effect⁴³ with magnetic insulators⁴⁴, or ferro-

magnets^{45,46}. We note, that the chiral perturbation of the electron spin density manifests itself in various ways. For instance, probing the chiral spin textures induced on a surface by means of spin-polarized scanning tunneling microscopy⁴⁷ would be a new tool to access the parameters of the electron gas. The chiral spin pattern in the electron gas can also induce a chiral order of magnetic ions located either in the same material or in a different layer of a heterostructure due to proximity effect. Therefore, the phenomenon opens a way to record the information using magnetic skyrmions or similar chiral spin textures by electrical means. Finally, the topological Hall effect is generally expected in magnetic systems with spin-orbit interaction due to asymmetric scattering of electrons on chiral spin textures¹⁵ pinned to defects and other inhomogeneities. In particular, the considered mechanism could be responsible for the recently observed topological Hall effect in TI and DMS⁴⁸⁻⁵⁰.

The work has been supported by the Russian Science Foundation (Project 18-72-10111), the Russian Foundation of Basic Research (grant 18-02-00668), and the Academy of Finland (Grant No. 318500). K.S.D. and N.S.A. thank the Foundation for the Advancement of Theoretical Physics and Mathematics BASIS.

* Electronic address: denisokonstantin@gmail.com

- ¹ X. G. Wen, F. Wilczek, and A. Zee, Phys. Rev. B **39**, 11413 (1989).
- ² X. Chen, Z.-C. Gu, and X.-G. Wen, Physical review b **82**, 155138 (2010).
- ³ C. D. Batista, S.-Z. Lin, S. Hayami, and Y. Kamiya, Reports on Progress in Physics **79**, 084504 (2016).
- ⁴ C. Kallin and J. Berlinsky, Reports on Progress in Physics **79**, 054502 (2016).
- ⁵ V. Kalmeyer and R. B. Laughlin, Phys. Rev. Lett. **59**, 2095 (1987).
- ⁶ K. Yang, L. Warman, and S. Girvin, Physical review letters **70**, 2641 (1993).
- ⁷ A. Kitaev, Annals of Physics **321**, 2 (2006).
- ⁸ G. Volovik, JETP lett **103**, 140 (2016).
- ⁹ P. A. Lee and N. Nagaosa, Physical Review B **46**, 5621 (1992).
- ¹⁰ B. Bauer, L. Cincio, B. P. Keller, M. Dolfi, G. Vidal, S. Trebst, and A. W. Ludwig, Nature communications **5**, 5137 (2014).
- ¹¹ L. Messio, S. Bieri, C. Lhuillier, and B. Bernu, Phys. Rev. Lett. **118**, 267201 (2017).
- ¹² J. Ye, Y. B. Kim, A. J. Millis, B. I. Shraiman, P. Majumdar, and Z. Tešanović, Phys. Rev. Lett. **83**, 3737 (1999).
- ¹³ S. Chun, M. Salamon, Y. Lyanda-Geller, P. Goldbart, and P. Han, Physical review letters **84**, 757 (2000).
- ¹⁴ P. Bruno, V. K. Dugaev, and M. Taillefumier, Phys. Rev. Lett. **93**, 096806 (2004).
- ¹⁵ K. Denisov, I. Rozhansky, N. Averkiev, and E. Lähderanta, Physical Review B **98**, 195439 (2018).
- ¹⁶ K. Hamamoto, M. Ezawa, and N. Nagaosa, Phys. Rev. B **92**, 115417 (2015).

- ¹⁷ A. Fert, N. Reyren, and V. Cros, Nature Reviews Materials **2**, 17031 (2017).
- ¹⁸ R. Wiesendanger, Nature Reviews Materials **1**, 16044 (2016).
- ¹⁹ A. Soumyanarayanan, M. Raju, A. G. Oyarce, A. K. Tan, M.-Y. Im, A. P. Petrović, P. Ho, K. Khoo, M. Tran, C. Gan, et al., Nature materials **16**, 898 (2017).
- ²⁰ T. Nakajima, H. Oike, A. Kikkawa, E. P. Gilbert, N. Booth, K. Kakurai, Y. Taguchi, Y. Tokura, F. Kagawa, and T.-h. Arima, Science advances **3**, e1602562 (2017).
- ²¹ X. Yu, W. Koshibae, Y. Tokunaga, K. Shibata, Y. Taguchi, N. Nagaosa, and Y. Tokura, Nature **564**, 95 (2018).
- ²² Y. Tokura, K. Yasuda, and A. Tsukazaki, Nature Reviews Physics **1**, 126 (2019).
- ²³ Y. Okada, C. Dhital, W. Zhou, E. D. Huemiller, H. Lin, S. Basak, A. Bansil, Y.-B. Huang, H. Ding, Z. Wang, et al., Phys. Rev. Lett. **106**, 206805 (2011).
- ²⁴ P. Wei, F. Katmis, B. A. Assaf, H. Steinberg, P. Jarillo-Herrero, D. Heiman, and J. S. Moodera, Phys. Rev. Lett. **110**, 186807 (2013).
- ²⁵ Y. Chen, J.-H. Chu, J. Analytis, Z. Liu, K. Igarashi, H.-H. Kuo, X. Qi, S.-K. Mo, R. Moore, D. Lu, et al., Science **329**, 659 (2010).
- ²⁶ I. M. Miron, G. Gaudin, S. Auffret, B. Rodmacq, A. Schuhl, S. Pizzini, J. Vogel, and P. Gambardella, Nature materials **9**, 230 (2010).
- ²⁷ I. M. Miron, K. Garello, G. Gaudin, P.-J. Zermatten, M. V. Costache, S. Auffret, S. Bandiera, B. Rodmacq, A. Schuhl, and P. Gambardella, Nature **476**, 189 (2011).
- ²⁸ A. Manchon, H. C. Koo, J. Nitta, S. Frolov, and R. Duine, Nature materials **14**, 871 (2015).
- ²⁹ L. Zhou, H. Song, K. Liu, Z. Luan, P. Wang, L. Sun,

- S. Jiang, H. Xiang, Y. Chen, J. Du, et al., *Science advances* **4**, eaao3318 (2018).
- ³⁰ C.-X. Liu, X.-L. Qi, X. Dai, Z. Fang, and S.-C. Zhang, *Physical review letters* **101**, 146802 (2008).
- ³¹ R. Yu, W. Zhang, H.-J. Zhang, S.-C. Zhang, X. Dai, and Z. Fang, *Science* **329**, 61 (2010).
- ³² A. Chernyshov, M. Overby, X. Liu, J. K. Furdyna, Y. Lyanda-Geller, and L. P. Rokhinson, *Nature Physics* **5**, 656 (2009).
- ³³ E. Novik, A. Pfeuffer-Jeschke, T. Jungwirth, V. Latussek, C. Becker, G. Landwehr, H. Buhmann, and L. Molenkamp, *Physical Review B* **72**, 035321 (2005).
- ³⁴ T. Jungwirth, J. Wunderlich, V. Novák, K. Olejnik, B. Gallagher, R. Campion, K. Edmonds, A. Rushforth, A. Ferguson, and P. Němec, *Reviews of Modern Physics* **86**, 855 (2014).
- ³⁵ H. Li, X. Wang, F. Doan, and A. Manchon, *Applied Physics Letters* **102**, 192411 (2013).
- ³⁶ E. H. Hwang and S. Das Sarma, *Phys. Rev. B* **75**, 205418 (2007).
- ³⁷ B. Wunsch, T. Stauber, F. Sols, and F. Guinea, *New Journal of Physics* **8**, 318 (2006).
- ³⁸ J.-J. Zhu, D.-X. Yao, S.-C. Zhang, and K. Chang, *Phys. Rev. Lett.* **106**, 097201 (2011).
- ³⁹ J. G. Checkelsky, J. Ye, Y. Onose, Y. Iwasa, and Y. Tokura, *Nature Physics* **8**, 729 (2012).
- ⁴⁰ J. A. Gaj and J. Kossut, **144**, 27 (2010).
- ⁴¹ X. Kou, W. Jiang, M. Lang, F. Xiu, L. He, Y. Wang, Y. Wang, X. Yu, A. Fedorov, P. Zhang, et al., *Journal of Applied Physics* **112**, 063912 (2012).
- ⁴² M. Watson, L. Collins-McIntyre, L. Shelford, A. I. Coldea, D. Prabhakaran, S. Speller, T. Mousavi, C. R. M. Grovenor, Z. Salman, S. Giblin, et al., *New Journal of Physics* **15**, 103016 (2013).
- ⁴³ I. Žutić, A. Matos-Abiague, B. Scharf, H. Dery, and K. Belashchenko, *Materials Today* (2018).
- ⁴⁴ I. Vobornik, U. Manju, J. Fujii, F. Borgatti, P. Torelli, D. Krizmancic, Y. S. Hor, R. J. Cava, and G. Panaccione, *Nano letters* **11**, 4079 (2011).
- ⁴⁵ Y. Lv, J. Kally, D. Zhang, J. S. Lee, M. Jamali, N. Samarth, and J.-P. Wang, *Nature communications* **9**, 111 (2018).
- ⁴⁶ J. S. Lee, A. Richardella, R. D. Fraleigh, C.-x. Liu, W. Zhao, and N. Samarth, *npj Quantum Materials* **3**, 51 (2018).
- ⁴⁷ R. Wiesendanger, *Rev. Mod. Phys.* **81**, 1495 (2009).
- ⁴⁸ J. Jiang, D. Xiao, F. Wang, J.-H. Shin, D. Andreoli, J. Zhang, R. Xiao, Y.-F. Zhao, M. Kayyalha, L. Zhang, et al., *arXiv preprint arXiv:1901.07611* (2019).
- ⁴⁹ C. Liu, Y. Zang, W. Ruan, Y. Gong, K. He, X. Ma, Q.-K. Xue, and Y. Wang, *Phys. Rev. Lett.* **119**, 176809 (2017).
- ⁵⁰ L. N. Oveshnikov, V. A. Kulbachinskii, A. B. Davydov, B. A. Aronzon, I. V. Rozhansky, N. S. Averkiev, K. I. Kugel, and V. Tripathi, *Scientific Reports* **5**, 17158 (2015).

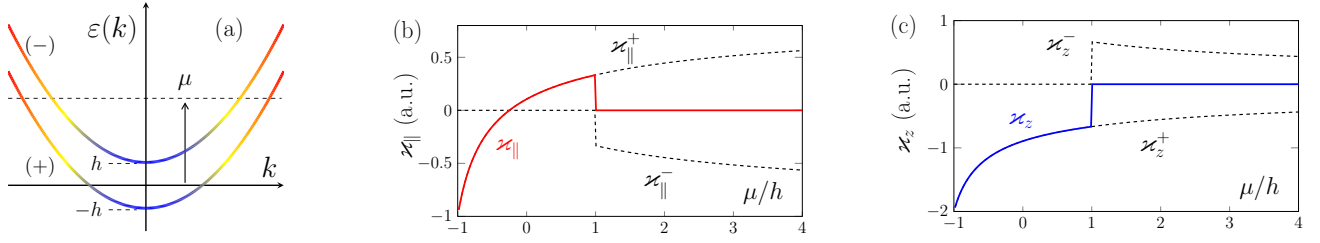


FIG. 2: (a) Parabolic-like electron spectrum Eq. 6, (b,c) the dependence of $\kappa_{\parallel,z}$ on μ for $\xi = 0.5$.

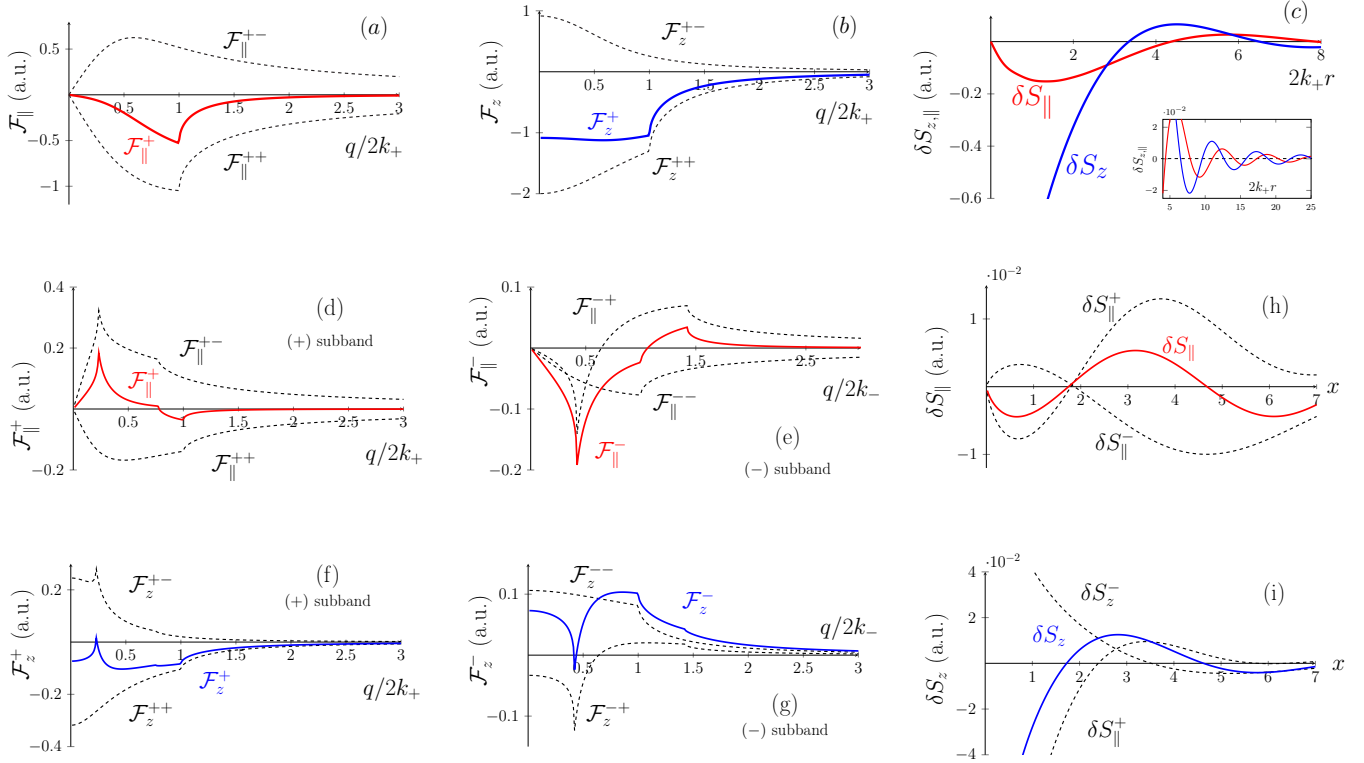


FIG. 3: (a,b,c) The dependence of $\mathcal{F}_{z,\parallel}^+$ on $q/2k_+$, and $\delta S_{z,\parallel}$ on $2k_+r$ in case of one filled spin subband ($\xi = 0.5$, $\mu = -0.4h$, $\zeta_+ = 1$), (d-g) the dependence of $\mathcal{F}_{z,\parallel}^{\pm}$ on $q/2k_{\pm}$, (h,i) the dependence of $\delta S_{z,\parallel}$ on $x = 2(\sqrt{2m\mu})r$ in case of two filled spin subbands, the parameters are $\mu = 3.5h$, $\xi = 0.5$, $\zeta_+ = 2.5$, $\zeta_- = 1.4$.

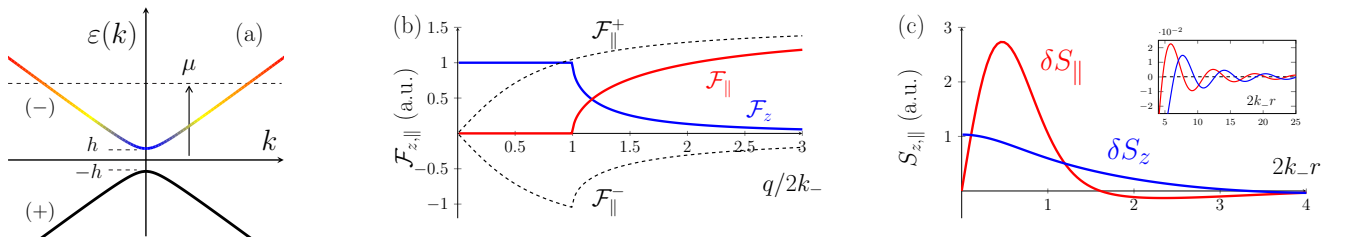


FIG. 4: (a) Dirac electron spectrum, (b) the dependence of $\mathcal{F}_{z,\parallel}^{\pm}$ on $q/2k_-$, (c) the dependence of $\delta S_{\parallel,z}$ on $2k_-r$, the inset shows the Friedel's oscillations. The parameters are $\mu = 2h$, $\zeta_- = 1.7$, $ak_- = 0.3$.

ONLINE SUPPORTING INFORMATION

Appendix A: The spin-density response functions for the parabolic-like spectrum.

Here we provide the derived analytical formulas for the spin-density response functions $\mathcal{F}_{z,\parallel}^{\pm}(q)$ in case of the electron parabolic-like spectrum $\varepsilon_k^{\pm} = k^2/2m \mp \sqrt{h^2 + (\lambda k)^2}$ (see Fig. 2a, Eq. 6 and the notation used in the main text). In the formulas below we use the following parameters: $\xi = m\lambda^2/h < 1$, $\zeta_{\pm} = \lambda k_{\pm}/h$, k_{\pm} is the Fermi wavevector in the corresponding subband, $a_0 = \lambda/2h$ has a dimensionality of length. We find that $\mathcal{F}_{z,\parallel}^{\pm}(q)$ are decomposed onto the intra- and interband contributions as $\mathcal{F}_{z,\parallel}^{\pm} = \mathcal{F}_{z,\parallel}^{\pm\pm} + \mathcal{F}_{z,\parallel}^{\pm\mp}$. The intraband terms $\mathcal{F}_{z,\parallel}^{\pm\pm}(q)$ are given by:

$$\begin{aligned} \mathcal{F}_{\parallel}^{\pm\pm}(q) &= \frac{m}{4\pi} \frac{1}{y(q)} \left(\Theta[2k_{\pm} - q] \Phi_1(q) + \Theta[q - 2k_{\pm}] \Phi_2^{\pm}(q) - \Phi_3^{\pm}(q) \right), \\ y(q) &= \sqrt{1 + (qa_0)^2 - \xi^2}, \quad \Phi_1(q) = \ln \sqrt{1 + (qa_0)^2}, \quad \Phi_3^{\pm}(q) = \tanh^{-1} \left(\frac{qa_0}{y(q)} \right) + \ln \frac{y(q) \pm \xi(qa_0)}{\sqrt{1 - \xi^2}}, \\ \Phi_2^{\pm}(q) &= \tanh^{-1} \left(\frac{a_0}{y(q)} \sqrt{q^2 - 4k_{\pm}^2} \right) + \ln \left[y(q) \sqrt{1 + \zeta_{\pm}^2} \pm \xi a_0 \sqrt{q^2 - 4k_{\pm}^2} \right] - \frac{1}{2} \ln [1 + \zeta_{\pm}^2 - \xi^2]. \end{aligned} \quad (\text{A1})$$

$$\begin{aligned} \mathcal{F}_z^{\pm\pm}(q) &= \mp \frac{m}{4\pi} \frac{1}{y(q)} \frac{\xi}{qa_0} \left(\Theta[2k_{\pm} - q] \Lambda_1^{\pm}(q) + \Theta[q - 2k_{\pm}] \Lambda_2^{\pm}(q) - \Lambda_3^{\pm}(q) \right), \\ \Lambda_1^{\pm}(q) &= y(q) \frac{\pi}{2\xi} \mp \ln \sqrt{1 + (qa_0)^2}, \quad \Lambda_3^{\pm}(q) = \frac{y(q)}{\xi} \tan^{-1} \left(\frac{1}{qa_0} \right) \mp \ln \left[1 + qa_0 \frac{y(q) + qa_0}{1 \mp \xi} \right], \\ \Lambda_2^{\pm}(q) &= \frac{y(q)}{\xi} \tan^{-1} \left(\frac{1}{a_0} \sqrt{\frac{1 + \zeta_{\pm}^2}{q^2 - 4k_{\pm}^2}} \right) \mp \left(\ln \left[1 + (qa_0)^2 + y(q) a_0 \sqrt{q^2 - 4k_{\pm}^2} \mp \xi \sqrt{1 + \zeta_{\pm}^2} \right] - \ln \left[\sqrt{1 + \zeta_{\pm}^2} \mp \xi \right] \right), \end{aligned} \quad (\text{A2})$$

and $\Theta[x]$ is the Heaviside function. The interband terms experience an additional symmetry $\mathcal{F}_z^{\pm\mp} = \mathcal{F}_{\parallel}^{\pm\mp}(2m\lambda/q)$. The functions $\mathcal{F}_{\parallel}^{\pm\mp}(q)$ are given by:

$$\begin{aligned} \mathcal{F}_{\parallel}^{+-}(q) &= \frac{m}{4\pi} \frac{1}{y(q)} \times \begin{cases} \mathcal{J}_+(q, 1), & \zeta_+ < 2\sqrt{\xi + \xi^2} \\ \Theta[q_1^+ - q] \mathcal{J}_+(q, 1) + \Theta[q - q_1^+] \Theta[q_2^+ - q] \mathcal{J}_+(q, x_+(q)) + \Theta[q - q_2^+] \mathcal{J}_+(q, 1), & \zeta_+ > 2\sqrt{\xi + \xi^2} \end{cases} \\ \mathcal{F}_{\parallel}^{-+}(q) &= \frac{m}{4\pi} \frac{1}{y(q)} \left(\Theta[q_1^- - q] \mathcal{J}_-(q, 1) + \Theta[q - q_1^-] \Theta[q_2^- - q] \mathcal{J}_-(q, |x_-(q)|) + \Theta[q - q_2^-] \mathcal{J}_-(q, 1) \right), \\ \mathcal{J}_{\pm}(q, x) &= [\text{sgn}(q - q_0)]^{\frac{(1\mp 1)}{2}} \ln \left[\frac{1 + \sqrt{F_{\pm}(q, 0)} \Delta_{\pm}(x)}{1 + \sqrt{F_{\pm}(q, x)} \Delta_{\pm}(0)} \right], \quad q_0 = \frac{1}{a_0} \sqrt{\xi + \xi^2}, \\ F_{\pm}(q, x) &= 1 + \xi \left(\frac{\Delta_{\pm}(x)}{y(q)} \right)^2 \left[\left(\frac{2k_{\pm}}{q} \right)^2 - \left(\frac{\zeta_{\pm}}{\xi} \right)^2 \right], \quad \Delta_{\pm}(x) = \frac{\xi}{\zeta_{\pm}^2} \left[\xi \mp \sqrt{1 + \zeta_{\pm}^2 x^2} \right], \\ q_{1,2}^{\pm} &= k_{\pm} [(-1)^{1,2}]^{\frac{(1\mp 1)}{2}} \left(1 + (-1)^{1,2} \sqrt{1 + 4\Delta_{\pm}(1)} \right), \quad x_{\pm}(q) = \text{Re} \left[\frac{q}{2k_{\pm}} \pm \frac{2m\lambda}{\zeta_{\pm}} \frac{y(q)}{\sqrt{q^2 - (2m\lambda)^2}} \right]. \end{aligned} \quad (\text{A3})$$

The dependence of $\mathcal{F}_{z,\parallel}^{\pm}(q)$ on q is shown in Fig. 3 and is thoughtfully discussed in the main text. In the limit of $q \rightarrow 0$ these functions behave as $\mathcal{F}_z^{\pm}(q) \approx \varkappa_z^{\pm}$, and $\mathcal{F}_{\parallel}^{\pm}(q) \approx q \cdot \varkappa_{\parallel}^{\pm}$, the coefficients $\varkappa_{z,\parallel}^{\pm}$ describing the local coupling regime are found to be:

$$\varkappa_z^{\pm} = \mp \frac{m}{4\pi} \frac{\Theta[\mu \pm h]}{\sqrt{1 + \zeta_{\pm}^2 \mp \xi}}, \quad \varkappa_{\parallel}^{\pm} = \pm \frac{1}{8\pi\lambda} \left(1 - \frac{1}{\sqrt{1 + \zeta_{\pm}^2 \mp \xi}} \right) \Theta[\mu \pm h]. \quad (\text{A4})$$

Appendix B: Derivation of spin-density response functions.

We consider a two-dimensional electron gas with an effective magnetic field acting on an electron spin in k -space: $\mathbf{B}_k = (\lambda k \cos(\chi\varphi_k + \gamma), \lambda k \sin(\chi\varphi_k + \gamma), h)$, where $(\lambda, h) > 0$, $\chi = \pm 1$, γ is an arbitrary real number. There are two spin subbands $s = \pm$, an electron in state (\mathbf{k}, s) has its spin \mathbf{S}_k^\pm parallel ($s = +$) or antiparallel ($s = -$) to \mathbf{B}_k . The corresponding spinors $|u_k^s\rangle$ for (\mathbf{k}, s) states are given:

$$\begin{aligned} |u_k^+\rangle &= \begin{pmatrix} e^{-i(\chi\varphi_k + \gamma)} a_k \\ b_k \end{pmatrix}, & |u_k^-\rangle &= \begin{pmatrix} b_k \\ -e^{i(\chi\varphi_k + \gamma)} a_k \end{pmatrix}, \\ a_k &= \sqrt{\frac{1+n_k}{2}} = \frac{h+B_k}{\sqrt{(\lambda k)^2 + (h+B_k)^2}}, & b_k &= \sqrt{\frac{1-n_k}{2}} = \frac{\lambda k}{\sqrt{(\lambda k)^2 + (h+B_k)^2}}, \end{aligned} \quad (\text{B1})$$

where $n_k = h/B_k$, and $B_k = \sqrt{h^2 + (\lambda k)^2}$. The static spin-density response functions $\mathcal{F}_\alpha(\mathbf{q})$ introduced in the main text Eq. 2 contain contributions from each spin subband and are given by:

$$\mathcal{F}_\alpha(\mathbf{q}) = \mathcal{F}_\alpha^+(\mathbf{q}) + \mathcal{F}_\alpha^-(\mathbf{q}), \quad \mathcal{F}_\alpha^s(\mathbf{q}) = \sum_{k, s'=\pm} f_k^s \left(\frac{\langle u_k^s | \hat{S}_\alpha | u_{k+q}^{s'} \rangle \langle u_{k+q}^{s'} | u_k^s \rangle}{\varepsilon_k^s - \varepsilon_{k+q}^{s'} + i0} + \frac{\langle u_{k-q}^{s'} | \hat{S}_\alpha | u_k^s \rangle \langle u_k^s | u_{k-q}^{s'} \rangle}{\varepsilon_k^s - \varepsilon_{k-q}^{s'} - i0} \right), \quad (\text{B2})$$

where $\hat{S}_\alpha = \hat{\sigma}_\alpha/2$, $\hat{\sigma}_\alpha$ is the Pauli matrix, $\alpha = (x, y, z)$, f_k^s and ε_k^s are the distribution function and an electron energy in state (\mathbf{k}, s) . Replacing $\mathbf{k} \rightarrow -\mathbf{k}$ in the last integral (we assume that $\varepsilon_k^s = \varepsilon_{-k}^s$) and using the following relations:

$$\begin{aligned} \langle u_{-k-q}^{s'} | \hat{S}_z | u_{-k}^s \rangle \langle u_{-k}^s | u_{-k-q}^{s'} \rangle &= \langle u_{k+q}^{s'} | \hat{S}_z | u_k^s \rangle \langle u_k^s | u_{k+q}^{s'} \rangle, \\ \langle u_{-k-q}^{s'} | \hat{S}_{x,y} | u_{-k}^s \rangle \langle u_{-k}^s | u_{-k-q}^{s'} \rangle &= -\langle u_{k+q}^{s'} | \hat{S}_{x,y} | u_k^s \rangle \langle u_k^s | u_{k+q}^{s'} \rangle, \end{aligned} \quad (\text{B3})$$

we get for the response functions at zero temperature:

$$\begin{aligned} \mathcal{F}_\alpha^s(\mathbf{q}) &= \int_0^{k_s} \frac{k dk}{2\pi} \mathcal{P} \int_0^{2\pi} \frac{d\theta}{2\pi} \sum_{s'=\pm} \frac{\mathcal{L}_{\alpha, kq}^{ss'}}{\varepsilon_k^s - \varepsilon_{k+q}^{s'}}, \\ \mathcal{L}_{z, kq}^{ss'} &= \text{Re} \left[\langle u_k^s | \hat{\sigma}_z | u_{k+q}^{s'} \rangle \langle u_{k+q}^{s'} | u_k^s \rangle \right], \quad \mathcal{L}_{xy, kq}^{ss'} = i \times \text{Im} \left[\langle u_k^s | \hat{\sigma}_{x,y} | u_{k+q}^{s'} \rangle \langle u_{k+q}^{s'} | u_k^s \rangle \right], \end{aligned} \quad (\text{B4})$$

where \mathcal{P} stands for the principal value, θ is the polar angle between \mathbf{k} and \mathbf{q} , k_\pm is the Fermi wavevector in s subband. We note that $\mathcal{L}_{xy, kq}^{ss'}$ are purely imaginary. It follows from the structure of $\mathcal{L}_{xy, kq}^{ss'}$, that the response functions $\mathcal{F}_{x,y}^s(\mathbf{q})$ for the in-plane spin components can be presented in form:

$$\mathcal{L}_{xy, kq}^{ss'} = i(\hat{n}\mathbf{e}_q)_{x,y} \mathcal{L}_{\parallel, kq}^{ss'}, \quad \mathcal{F}_{x,y}^s(\mathbf{q}) = i(\hat{n}\mathbf{e}_q)_{x,y} \mathcal{F}_{\parallel}^s(q), \quad (\text{B5})$$

$$\mathcal{F}_{\parallel}^s(q) = \int_0^{k_s} \frac{k dk}{2\pi} \mathcal{P} \int_0^{2\pi} \frac{d\theta}{2\pi} \sum_{s'=\pm} \frac{\mathcal{L}_{\parallel, kq}^{ss'}}{\varepsilon_k^s - \varepsilon_{k+q}^{s'}}, \quad \hat{n} = \begin{pmatrix} \sin \gamma & (-1)^x \cos \gamma \\ -\cos \gamma & (-1)^x \sin \gamma \end{pmatrix}, \quad (\text{B6})$$

where \hat{n} is an orthogonal matrix determined by a particular spin-orbit interaction type, $\mathbf{e}_q = \mathbf{q}/q$ is the unit vector in the direction of \mathbf{q} , the functions $\mathcal{F}_{\parallel}^\pm(q)$ are real and depend only on q modulus. The explicit expressions for the matrix elements $\mathcal{L}_{z, \parallel, kq}^{ss'}$ are given:

$$\mathcal{L}_{z, kq}^{ss'} = \frac{(-1)^{\frac{(1-s)}{2}}}{2} (n_k + (-1)^{s-s'} n_{k+q}), \quad \mathcal{L}_{\parallel, kq}^{ss'} = (-1)^{s-s'} (qa_0) n_k n_{k+q}, \quad a_0 = \frac{\lambda}{2h}. \quad (\text{B7})$$

When calculating these matrix elements the following relation is very useful: $(a_k b_k)/(a_k^2 - b_k^2) = ka_0$. The details of the spin-density response depend on a particular electron spectrum, below we provide the calculations for parabolic-like and Dirac types of spectra.

1. Integrals for the Dirac spectrum

Here we present the calculations of $\mathcal{F}_{z,\parallel}^{\pm}(q)$ for the Dirac electron spectrum $\varepsilon_k^{\pm} = \mp B_k = \mp\sqrt{h^2 + (\lambda k)^2}$, see Eq. 7 and Fig.4a in the main text. We write the spin-density response functions in form:

$$\begin{aligned} \begin{pmatrix} \mathcal{F}_{\parallel}^s(q) \\ \mathcal{F}_z^s(q) \end{pmatrix} &= - \int_0^{k_s} \frac{k dk}{2\pi} \mathcal{P} \int_0^{2\pi} \frac{d\theta}{2\pi} \begin{pmatrix} s\mathcal{A}_{k,q} \times (qa_0) \\ \mathcal{B}_{k,q} \end{pmatrix}, \\ \mathcal{A}_{k,q} &= \left[\frac{1}{B_k - B_{k+q}} - \frac{1}{B_k + B_{k+q}} \right] n_k n_{k+q} = -\frac{1}{q} \left(\frac{m_g}{B_k} \right) \frac{2h}{q + 2k \cos \theta}, \\ \mathcal{B}_{k,q} &= \frac{1}{2} \left[\frac{n_k + n_{k+q}}{B_k - B_{k+q}} + \frac{n_k - n_{k+q}}{B_k + B_{k+q}} \right] = -\frac{2h}{q + 2k \cos \theta}, \end{aligned} \quad (\text{B8})$$

where we introduced the parameter $m_g = h/\lambda^2$, which is an effective mass at the bottom of subband $k \approx 0$. The integral over the angle in Eq. B8 for both $\mathcal{F}_{z,\parallel}^s$ is taken using:

$$\mathcal{P} \int_0^{2\pi} \frac{d\theta}{2\pi} \frac{1}{a + b \cos \theta} = \frac{\Theta[a - b]}{\sqrt{a^2 - b^2}}, \quad a, b > 0. \quad (\text{B9})$$

The remaining integrals over k are taken using I_z for \mathcal{F}_z^s , and I_{\parallel} for $\mathcal{F}_{\parallel}^s$ correspondingly:

$$\begin{aligned} I_z &= \int_0^1 x dx \frac{\Theta[z - x]}{\sqrt{z^2 - x^2}} = z - \Theta[z - 1] \sqrt{z^2 - 1}, \\ I_{\parallel} &= \int_0^1 x dx \frac{1}{\sqrt{y^2 + x^2}} \frac{\Theta[z - x]}{\sqrt{z^2 - x^2}} = \tan^{-1} \left(\frac{z}{y} \right) - \Theta[z - 1] \tan^{-1} \left(\sqrt{\frac{z^2 - 1}{y^2 + 1}} \right). \end{aligned} \quad (\text{B10})$$

Let us consider the case when the Fermi energy $\mu > h$ lies in the upper subband (see Fig.4a). The response from partially filled ($-$) subband, using the integrals in Eq. (B9,B10), is given by:

$$\begin{aligned} \mathcal{F}_z^-(q) &= \frac{m_g}{4\pi} \left(1 - \Theta[q - 2k_-] \sqrt{1 - (q/2k_-)^2} \right), \\ \mathcal{F}_{\parallel}^-(q) &= -\frac{m_g}{4\pi} \left[\tan^{-1}(qa_0) - \Theta[q - 2k_-] \tan^{-1} \left(a_0 \sqrt{\frac{q^2 - 4k_-^2}{1 + \zeta_-^2}} \right) \right], \end{aligned} \quad (\text{B11})$$

here $\zeta_- = \lambda k_-/h$. Considering the response from the fully filled ($+$) subband we should take the integrals Eq. B10 in the limit $k_+ \rightarrow \infty$. At that no response of spin z -component is induced ($\mathcal{F}_z^+ = 0$), while the in-plane response function is given by:

$$\mathcal{F}_{\parallel}^+(q) = \frac{m_g}{4\pi} \tan^{-1}(qa_0). \quad (\text{B12})$$

2. Integrals for the parabolic-like spectrum

Here we present the calculations of $\mathcal{F}_{z,\parallel}^{\pm}(q)$ for the parabolic-like electron spectrum $\varepsilon_k^{\pm} = k^2/2m \mp \sqrt{h^2 + (\lambda k)^2}$, see Eq. 6 and Fig.2a in the main text. We write the spin-density response functions in form:

$$\begin{aligned} \begin{pmatrix} \mathcal{F}_{\parallel}^s(q) \\ \mathcal{F}_z^s(q) \end{pmatrix} &= \int_0^{k_s} \frac{kdk}{2\pi} \mathcal{P} \int_0^{2\pi} \frac{d\theta}{2\pi} \left(\mathcal{C}_{k,q}^s \times (qa_0) \right), & (B13) \\ \mathcal{C}_{k,q}^{\pm} &= \left[\frac{1}{(\delta\varepsilon_{k,q} \mp B_k) \pm B_{k+q}} - \frac{1}{(\delta\varepsilon_{k,q} \mp B_k) \mp B_{k+q}} \right] n_k n_{k+q} = \mp \frac{2hn_k}{(\delta\varepsilon_{k,q} \mp B_k)^2 - B_{k+q}^2} \\ \mathcal{D}_{k,q}^{\pm} &= \pm \frac{1}{2} \left[\frac{n_k + n_{k+q}}{(\delta\varepsilon_{k,q} \mp B_k) \pm B_{k+q}} + \frac{n_k - n_{k+q}}{(\delta\varepsilon_{k,q} \mp B_k) \mp B_{k+q}} \right] = \frac{\pm n_k \delta\varepsilon_{k,q} - 2h}{(\delta\varepsilon_{k,q} \mp B_k)^2 - B_{k+q}^2}, \\ \delta\varepsilon_{k,q} &= -\frac{q^2}{2m} - \frac{kq}{m} \cos\theta. \end{aligned}$$

The denominator in the $\mathcal{C}_{k,q}^{\pm}, \mathcal{D}_{k,q}^{\pm}$ can be expressed as $(\delta\varepsilon_{k,q} \mp B_k)^2 - B_{k+q}^2 = (kq/m)^2 \times (a_{\pm} + b_{\pm} \cos\theta + \cos^2\theta)$, where the coefficients a_{\pm}, b_{\pm} do not depend on θ . There are two types of integrals with respect to the angle θ :

$$I_1^{\pm} = \mathcal{P} \int_0^{2\pi} \frac{d\theta}{2\pi} \frac{1}{a_{\pm} + b_{\pm} \cos\theta + \cos^2\theta} = \pm \frac{x^2 t}{|\Delta_{\pm}(x)|} \left[\frac{1}{w(t,x)} - \frac{\text{sgn}(u_{\pm}(x,t))}{w(u_{\pm},x)} \right], \quad (B14)$$

$$I_2^{\pm} = \mathcal{P} \int_0^{2\pi} \frac{d\theta}{2\pi} \frac{\cos\theta}{a_{\pm} + b_{\pm} \cos\theta + \cos^2\theta} = \pm \frac{xt}{|\Delta_{\pm}(x)|} \left[\text{sgn}(u_{\pm}(x,t)) \frac{u_{\pm}(x,t)}{w(u_{\pm},x)} - \frac{t}{w(t,x)} \right], \quad (B15)$$

where we introduced the following notation: $x = k/k_{\pm}, t = q/2k_{\pm}$, the functions $\Delta_{\pm}(x), u_{\pm}(x,t), w(t,x)$ are given by:

$$\Delta_{\pm}(x) = \frac{\xi}{\zeta_{\pm}^2} \left[\xi \mp \sqrt{1 + x^2 \zeta_{\pm}^2} \right] \leq 0, \quad u_{\pm}(x,t) = t - \frac{\Delta_{\pm}(x)}{t}, \quad w(t,x) = \text{Re} \left[\sqrt{t^2 - x^2} \right] = \Theta(|t| - x) \sqrt{t^2 - x^2},$$

here $\xi = m\lambda^2/h, \zeta_{\pm} = \lambda k_{\pm}/h$. For the calculation of $\mathcal{F}_{\parallel}^{\pm}$ we need only I_1^{\pm} integrals, while calculating \mathcal{F}_z^{\pm} requires both $I_{1,2}^{\pm}$. After the integration over the angle we can decompose the integrals over k as $\mathcal{F}_{\parallel,z}^{\pm}(t) = \mathcal{F}_{\parallel,z}^{\pm\pm}(t) + \mathcal{F}_{\parallel,z}^{\pm\mp}(t)$, where

$$\mathcal{F}_{\parallel}^{\pm\pm}(t) = -Q_{\pm} \mathcal{I}_1^{\pm}, \quad \mathcal{F}_z^{\pm\pm}(t) = \mp Q_{\pm} \frac{1}{qa_0} \mathcal{I}_2^{\pm}, \quad \mathcal{F}_{\parallel}^{\pm\mp}(t) = \left(\frac{q}{2m\lambda} \right) \mathcal{F}_z^{\pm\mp}(t) = Q_{\pm} \mathcal{I}_3^{\pm}, \quad (B16)$$

here the pre-factor $Q_{\pm} = (m/4\pi)(m\lambda/k_{\pm})$, the integrals $\mathcal{I}_{1,2,3}^{\pm}$ are shown below:

$$\mathcal{I}_1^{\pm} = \int_0^1 \frac{xdx}{|\Delta_{\pm}(x)|} \frac{\Theta[t-x]}{\sqrt{t^2-x^2}} \frac{1}{\sqrt{1+\zeta_{\pm}^2 x^2}}, \quad (B17)$$

$$\mathcal{I}_2^{\pm} = \int_0^1 \frac{xdx}{|\Delta_{\pm}(x)|} \frac{\Theta[t-x]}{\sqrt{t^2-x^2}}, \quad (B18)$$

$$\mathcal{I}_3^{\pm} = \int_0^1 \frac{xdx}{|\Delta_{\pm}(x)|} \frac{\Theta[|u_{\pm}(x,t)|-x] \text{sgn}[u_{\pm}(x,t)]}{\sqrt{u_{\pm}^2(x,t)-x^2} \sqrt{1+\zeta_{\pm}^2 x^2}}. \quad (B19)$$

The terms $\mathcal{F}_{\parallel,z}^{\pm\pm}, \mathcal{F}_{\parallel,z}^{\pm\mp}$ listed in the Appendix A are reproduced after some straightforward calculations of $\mathcal{I}_{1,2,3}^{\pm}$ given above. Let us only note the complex range of integration in \mathcal{I}_3^{\pm} , which leads to a double spike structure of the the interband response functions. This feature reflects the presence of two nesting vectors of the Fermi surface at the interband transitions.